Accepted Manuscript File

S. Sharifi Golru, A.S. May, <u>E.J. Biddinger*</u>, "Modifying Copper Local Environment with Electrolyte Additives to Alter CO₂ Electroreduction vs Hydrogen Evolution," *ACS Catalysis*, 13 (2023), 7831-7843. https://doi.org/10.1021/acscatal.3c00035

Modifying copper local environment with electrolyte additives to alter CO₂ electroreduction versus hydrogen evolution

Samaneh Sharifi Golru^{1,2}, Andrew S. May¹, Elizabeth J. Biddinger^{1,2,*}

ABSTRACT

CO₂ electroreduction (CO2ER) by using renewable energy resources is a promising method to mitigate the CO₂ level in the atmosphere as well as producing valuable chemicals. Local environment at the electrode-electrolyte interface plays a key role in CO2ER activity and selectivity along with its competing hydrogen evolution reaction (HER). In addition to the catalyst and reactor design, electrolyte has also a significant impact on the interface. Herein, electrolyte additives were used to modify the local environment around the Cu catalyst during CO2ER. To this purpose, 10mM of ionic additives with bis(trifluoromethylsulfonyl)imide ([NTF₂]⁻) and dicyanamide ([DCA]⁻) as anions and 1-butyl-3-methylimidazolium ([BMIM]⁺), potassium (K⁺), or sodium (Na⁺) as cations have been added to an aqueous potassium bicarbonate solution (0.1 M KHCO₃). COMSOL Multiphysics was also used to calculate the local pH and CO₂ concentration at electrode-electrolyte interface in different electrolytes. Results showed that the local environment modifications by the electrolyte additives altered the activity and selectivity of Cu in CO2ER. It was found that the CO2ER activity at -0.92 V was enhanced when using anion with high CO₂ affinity and high hydrophobicity such as [NTF₂]. Among [NTF₂]-based additives, [BMIM][NTF₂] had a higher faradaic efficiency (FE) for formate (38.7%) compared to K[NTF₂] (23.2%) and Na[NTF₂] (18.5%) at -0.92 V likely due to the presence of imidazolium cation which can further stabilize the intermediates on the surface and enhance CO2ER. Electrolytes containing [DCA]-based additives with high hydrophilicity and low CO₂ affinity had a very high HER selectivity (>90% FE_{H2}) and low CO2ER selectivity regardless of the cation nature. This observation is attributed to the presence of hydrophilic [BMIM][DCA] in the vicinity of the

¹ Department of Chemical Engineering, The City College of New York, CUNY, New York (USA)

² Ph.D. Program in Chemistry, The Graduate Center of the City University of New York, New York (USA)

^{*}Corresponding Author: [E-mail: ebiddinger@ccny.cuny.edu]

catalyst which impacts the microenvironment around the catalyst. We observed that [DCA]⁻ anions have a high affinity to adsorb on Cu catalysts as soon as the catalyst is submerged in the electrolyte. Although FTIR showed that [DCA]⁻ anions desorb from the surface at negative potentials, it is likely that [DCA]⁻ anions still remain in the proximity of the electrode, next to the adsorbed cations, impacting the transport of H₂O and CO₂, and altering the product selectivity. COMSOL calculations showed that the local pH is directly proportional to the H₂ evolution activity. Also, hydrophilic salts such as those with the [DCA]⁻ anion had a more alkaline local pH which leads to a lower CO₂ concentration in the vicinity of the catalyst.

Keywords: CO2 reduction, Cu electrodes, Ionic liquids, Electrocatalysis, COMSOL.

1. INTRODUCTION

The use of fossil fuels as the primary energy source has increased the CO₂ concentration in the atmosphere leading to global warming¹. CO₂ electroreduction (CO2ER) is a promising approach to mitigate the CO₂ level in the atmosphere which can simultaneously produce valuable chemicals and fuels^{2,3}. Besides catalyst⁴⁻⁶ and reactor design⁷⁻⁹, electrolyte also plays a key role in CO2ER¹⁰-¹². Among different electrolytes, aqueous solutions are the most common electrolytes for CO2ER due to their low cost, abundance, and eco-friendliness¹³⁻¹⁶. However, the product selectivity and activity in aqueous electrolytes are poor due to their low CO2 solubility and the presence of the competing hydrogen evolution reaction (HER). Using additives in aqueous electrolytes can be a promising method to tune the properties of the electrolyte and enhance CO2ER^{10, 14, 17-38}. The local environment at electrode-electrolyte interface is significantly impacted by the electrolyte. The molecules/ions in the electrolyte can impact CO2ER by blocking the active sites on the electrode, interacting with reactants and intermediates, altering the local electric filed and pH around the electrode^{12, 39, 40}. Varela et al. reported that adding 0.3 M KI to an aqueous electrolyte can enhance faradaic efficiency for methane (FE_{CH4}) on Cu¹⁰. They suggested that I⁻ anions are adsorbed on the surface and could facilitate the protonation of CO which is needed for CH₄ formation ¹⁰. Verma et al. also showed that CO2ER on Ag is suppressed in the presence of large anions such as Clwhich directly adsorb on the surface and destabilize the intermediates¹¹. In another study, Singh et al. also showed that the size of cation impacts the local pH¹². They reported that large cations at interface undergo hydrolysis and lower the local pH. This results in enhanced C₂ and CO formation on Cu and Ag electrodes, respectively¹².

We previously showed that the anion choice has a significant impact on CO2ER activity and selectivity with copper when using dilute ionic liquid (IL) additives in aqueous electrolytes¹⁸. We investigated 10mM of 1-butyl-3-methylimidazolium ([BMIM]⁺) cation-based ILs with five different anions as additives in 0.1M potassium bicarbonate (KHCO₃) electrolytes. The imidazolium cation was selected for reported stabilization of the CO₂ intermediates ^{20, 24, 30}, and anions were selected for their different CO₂ affinities and hydrophobicities. We observed that the CO2ER towards formate be significantly enhanced when could bis(trifluoromethylsulfonyl)imide ([NTF₂]) as the anion (FE_{formate} 38.7% at -0.92V vs. RHE)¹⁸. HER could be substantially promoted when using dicyanamide ([DCA]⁻) as the anion (FE_{H2} 92.9% at -0.92V vs. RHE). Our observations showed that partial current densities towards CO2ER products increased as the hydrophobicity and CO₂ affinity of the anion increased. More specifically, the highest and lowest CO2ER activity was observed for [BMIM][NTF2] (most hydrophobic) and [BMIM][DCA] (least hydrophobic), respectively 18. We hypothesized that the CO₂ affinity towards the IL additives and hydrophobicity of the IL, both of which are dictated by the anion choice, had the most significant roles in the interplay between CO2ER and its products, and the competing HER.

In this study, the local environment around Cu catalyst in the presence of ionic additives with 10 mM concentration was investigated to gain a deeper insight into the role of ions in the electrolyte. By minimizing the additive concentration to 10 mM, the negative impacts caused by viscosity increase such as mass transfer limitations are reduced. Additionally, with a small concentration of IL, the IL solubility limit in the aqueous electrolyte is not reached, especially for hydrophobic [NTF₂] anion. The diluted IL/water electrolytes also ensure enough water is available to produce hydrogen-containing CO2ER products. [NTF₂]-based salts with three cations (Na⁺, K⁺, and [BMIM]⁺), and [DCA]-based salts with two cations (Na⁺ and [BMIM]⁺) were used. Inorganic cations (Na⁺ and K⁺) are hydrated in the aqueous electrolytes due to their small size and their high charge density^{41, 42}. The hydration shell around the inorganic cations does not allow the cations to be specifically adsorbed on the electrode surface. However, bulky organic cations such as [BMIM]⁺ do not have the hydration shell due to their size and their hydrophobic nature. [BMIM]⁺ cations can interact with CO₂ molecules due to the presence of acidic hydrogen at C₂ position of the imidazolium ring⁴³⁻⁴⁵. When comparing ILs, the CO₂ affinity of the ILs is more dependent on the anion nature and cations has minimal impact on it⁴⁶. In order to study the

adsorption of ions on the catalyst surface, electrochemical quartz crystal microbalance (EQCM), XPS, and in situ-FTIR were utilized. COMSOL Multiphysics studies were also used to deeper probe the influence of ionic additives on the electrode-electrolyte interface observed experimentally.

2. EXPERIMENTAL SECTION

2.1. Electrode preparation

Polycrystalline Cu electrodes with 0.9 cm² geometric surface area were constructed of a 0.5 cm × 0.7 cm × 0.01 cm Cu foil (99.999%) connected to a 1.25 cm length by 0.5 mm diameter twisted Cu wire (99.999%). Electrodes were first electropolished in 1 M phosphoric acid (H₃PO₄) at 1.8 V in a two-electrode setup for 300 s. A Pt mesh electrode was used as counter electrode.

2.2. Electrochemical measurements

Electrochemical experiments such as cyclic voltammetry (CV), electrochemical impedance spectroscopy (EIS), and CO2ER were conducted in an H-type cell with a Nafion-212 membrane between the anodic and cathodic chambers. A Gamry Interface 1000 potentiostat was used for all electrochemical measurements. Cu electrode (0.9 cm²) was used as the working electrode. A platinum mesh and a BASi Ag/AgCl (3 M NaCl) were used as counter and reference electrodes, respectively. All experiments have been performed with same analyte which was 0.1 M potassium bicarbonate (KHCO₃, Fisher Chemical, Certified ACS). The catholyte was a solution of 0.1 M KHCO₃ with or without 10 mM of an IL or inorganic salt. Since the concentration of salt is very low (10 mM), these electrolytes are still considered as aqueous electrolytes and water was the main solvent in this study. It needs to be mentioned that minimizing the additive concentration to 10 mM helps reduce the mass transfer limitations, avoid the IL solubility limits especially for the hydrophobic [NTF₂] anion, and also provide enough water available to produce hydrogencontaining products in CO2ER. The ionic liquids (ILs) used in this study, [BMIM][NTF₂] and [BMIM][DCA], were purchased from Ionic Liquid Technologies (Io-Li-Tec) Inc. The inorganic salts, Na[NTF₂], K[NTF₂] and Na[DCA], were purchased from Alfa Aesar. Figure 1 shows the chemical structure of different anions and cations used in this study.

Cyclic voltammetry was performed in N₂ and CO₂- saturated electrolytes with a scan rate of 50 mV/s for 8 cycles from -1.0 V to -1.8 V vs. Ag/AgCl. Before each experiment, the electrolyte was

saturated by bubbling N_2 or CO_2 gas for 30 min. pH values of N_2 -saturated and CO_2 -saturated electrolytes were 9.3 and 6.8, respectively. Additives did not impact the electrolyte pH, since they were used at low concentrations (10 mM). EIS was also performed in CO_2 saturated electrolytes with the frequency range of 10 KHz to 0.1 Hz, 10 mV AC amplitude at -0.82 V and -1.09 V versus RHE. In order to reduce the oxides on the electrode surface, a pre-electrolysis at -1.02 V in CO_2 -saturated electrolyte was performed prior to the CO2ER experiments. CO2ER experiments were then performed on Cu electrodes at different potentials (-0.92 V, -1.02 V, and -1.12 V vs. RHE) for 30 mins. In addition to saturating the electrolyte with CO_2 before CO2ER, CO_2 gas with a flow rate of 35 ml/min was bubbled in the catholyte during CO2ER experiments. The potentials were corrected to reversible hydrogen electrode (RHE) by the equation $V_{vs.\ RHE} = V_{measuredvs.\ Ag/AgCl} + 0.209 +0.059 \ pH_{solution}$. The potentials mentioned in this article are versus RHE, unless otherwise noted. Current-interrupt iR compensation was used to correct for the ohmic resistance during the CO2ER experiments. All measurements were repeated at least three times to evaluate the reproducibility. Gaseous and liquid products were detected using MicroGC and NMR, respectively, according to the methods mentioned in our previous paper 18.

Cations	Anions
Na ⁺ K ⁺	F ₃ C S S CF ₃ [NTF ₂]
[BMIM] ⁺	NC ^O CN [DCA]⁻

Figure 1. Chemical structure of the cations and anions used in this study.

2.3. Electrochemical quartz crystal microbalance (EQCM)

In order to study the adsorption of the additives on the catalyst, LSV-EQCM experiments were performed in a EQCM static Teflon cell (purchased from GAMRY) which is connected to a GAMRY eQCM 10M quartz crystal microbalance paired with a GAMRY Interface 1000 potentiostat (Figure S3). A Cu-deposited quartz crystal, a platinum wire and Ag/AgCl (3M NaCl)

were used as the working, counter and reference electrodes, respectively. More information regarding EQCM experiments can be found in the Supporting Information (Figures S4, S5, and S6). The potential range was -0.5 to -1.8 V vs. Ag/AgCl with a scan rate of 20 mV/s. The frequency shift during LSV was recorded by EQCM instrument. The mass change was then calculated by Sauerbrey's equation (Eq. S1).

2.4. X-ray photoelectron spectroscopy (XPS)

The surface analysis of the catalysts after submerging in the additive-free and additive-containing electrolytes for 4 hrs with CO₂ sparging to reach saturation (with no potential applied), and also after CO2ER experiments at different potentials was performed by XPS using a Physical Electronics PHI 5000 VersaProbe II spectrometer with an Al Kα X-ray source (1486.6 eV). Before XPS experiments, electrodes were rinsed with DI water followed by drying at 40 °C in vacuum oven overnight. The binding energy of all spectra was calibrated with C1s peak at 284.8 eV.

2.5. Fourier-transform infrared spectroscopy (FTIR)

A VeeMAX III ATR (attenuated total reflection) from PIKE Technologies with 60° angled Si ATR crystals with a lab-built Teflon electrochemical cell were used to conduct the FTIR experiments on a ThermoScientific Nicolet is 50 FTIR bench. Thin Cu films were prepared on the Si ATR crystals via an electroless plating procedure similar to that done Gunathunge et al.⁴⁷. The ATR crystal reflecting surfaces were polished using a 0.05 micron alumina slurry followed by alternating sonication bathes in deionized (DI) water and acetone for 5 minutes. The crystals were submerged subsequently into 1 M ammonium fluoride for 60 seconds, a seed solution for 2 minutes, and a plating solution for 5 minutes. The seed solution consisted of 0.5 wt% hydrofluoric acid (HF) and 0.75 mM copper sulfate (CuSO₄) in DI water. The plating solution consisted of 250 mM formaldehyde (CH₂O), 20 mM CuSO₄, 20 mM disodium ethylenediaminetetraacetic acid (Na₂EDTA), 0.3 mM 2,2-bipyridine (C₁₀H₈N₂), adjusted to pH 12 using potassium hydroxide (KOH), all in DI water and heated to 55 °C for use. For electrochemical experiments, 7mL of electrolyte was placed into the electrochemical cell with Cu coated ATR crystal. CO₂ was bubbled into the cell until saturated and remained bubbling during the remainder of experiments. The counter electrode was a graphite rod placed into a capillary tube filled with 0.1M KHCO₃ with glass frit to separate from the working electrode. The reference electrode was an Ag/AgCl electrode from BASi. Background spectra were taken with the cell open to air before electrolyte

was added, with 64 co-added scans at a 4cm⁻¹ resolution. Spectra during LSV were taken with 16 co-added scans at a 4cm⁻¹ resolution. A liquid nitrogen cooled MCT detector was used for all spectra.

Safety Note for use of hydrofluoric acid (HF): Extra safety precautions were taken when using HF including working in an HF-designated chemical hood, and wearing butyl rubber gloves, rubberized apron and face shield. An HF safety and spill kit was readily available whenever HF was utilized. Researchers had to be specifically trained and approved for handling HF.

2.6. Modeling CO₂ electroreduction by COMSOL

In order to study the interfacial properties such as pH and concentration of species at the electrodeelectrolyte interface, the boundary layer in vicinity of the cathode was simulated by the method proposed by Hashiba et al.⁴⁸. More details regarding the COMSOL simulation have been provided in the SI (Figure S7, TableS2, and TableS3).

3. RESULTS AND DISCUSSION

3.1. Effect of ionic additives on the activity and selectivity of Cu catalysts

In order to obtain an insight into the role of additive ions in CO2ER, Na[NTF2], K[NTF2], and Na[DCA] were used as additive in 0.1 M KHCO3, and the results were compared with [BMIM][NTF2] and [BMIM][DCA] additives which were studied in our previous work¹⁸. Prior to CO2 electroreduction experiments, cyclic voltammetry measurements in N2- and CO2-saturated electrolytes were performed to evaluate the general activity of the Cu electrodes in different electrolytes. Figure 2 shows the CVs in N2- and CO2-saturated electrolytes containing [NTF2]⁻ and [DCA]⁻-based additives. CVs in N2-saturated electrolytes (Figure 2a-e) can provide an insight into the activity toward HER, as no CO2 is present in the electrolyte. According to Figure 2a-c, all [NTF2]⁻-based additives had a minimal impact on the HER onset potential and HER activity. However, [BMIM][NTF2] showed a lower HER activity compared to the inorganic salts (Na[NTF2] and K[NTF2]) at more negative potentials (<-0.9 V vs. RHE). This observation can be due to the competition between large cations and water molecules for an adsorption site on the electrode surface at high overpotentials⁴⁹⁻⁵¹. In contrast to [NTF2]⁻ salts, [DCA]⁻ salts significantly enhanced the HER activity (Figure 2d-e). Compared to the additive-free electrolyte and electrolytes containing [NTF2]⁻ additives, [DCA]⁻ salts (regardless of the cation nature) had a

much higher current density and a more positive onset potential in N₂-saturated electrolytes. Changing the cation did not impact the HER onset potential and the activity in less negative potentials (>-0.83 V vs. RHE) in [DCA]⁻ electrolytes. The impact of the cation at more negative potentials was also minimal. This observation can be indicative of the dominant role of the [DCA]⁻ anion in the electrolyte.

The general activity toward both CO2ER and HER reactions was also studied in CO₂-saturated electrolytes (Figure 2f-j). All of the [NTF₂]-containing electrolytes had a more positive onset potential and a higher activity for CO2ER at less negative potentials (>-1.07 V vs. RHE) compared to the additive-free electrolyte. Similar to what was observed in N₂-saturated electrolytes, the CO2ER activity for [BMIM][NTF₂] was lessened at higher potentials (<-1.07 V vs. RHE), likely due to the competition of the large IL, water and CO₂ for a position on the surface. In CO₂-saturated electrolytes containing [DCA]⁻ salts (Figure 2i-j), a more positive onset potential and a higher activity were observed compared to the additive free electrolyte. Moreover, it was found that [BMIM][DCA] additive had a more negative onset potential and a lower activity in CO₂-saturated electrolytes compared to Na[DCA]. This could be also due to the competition of CO₂ and water molecules with large organic cations to access the electrode surface. The higher activity in [DCA]⁻ salts compared to [NTF₂]⁻ salts and additive-free electrolytes in both N₂- and CO₂- saturated is most probably due to the enhanced HER rather than CO2ER.

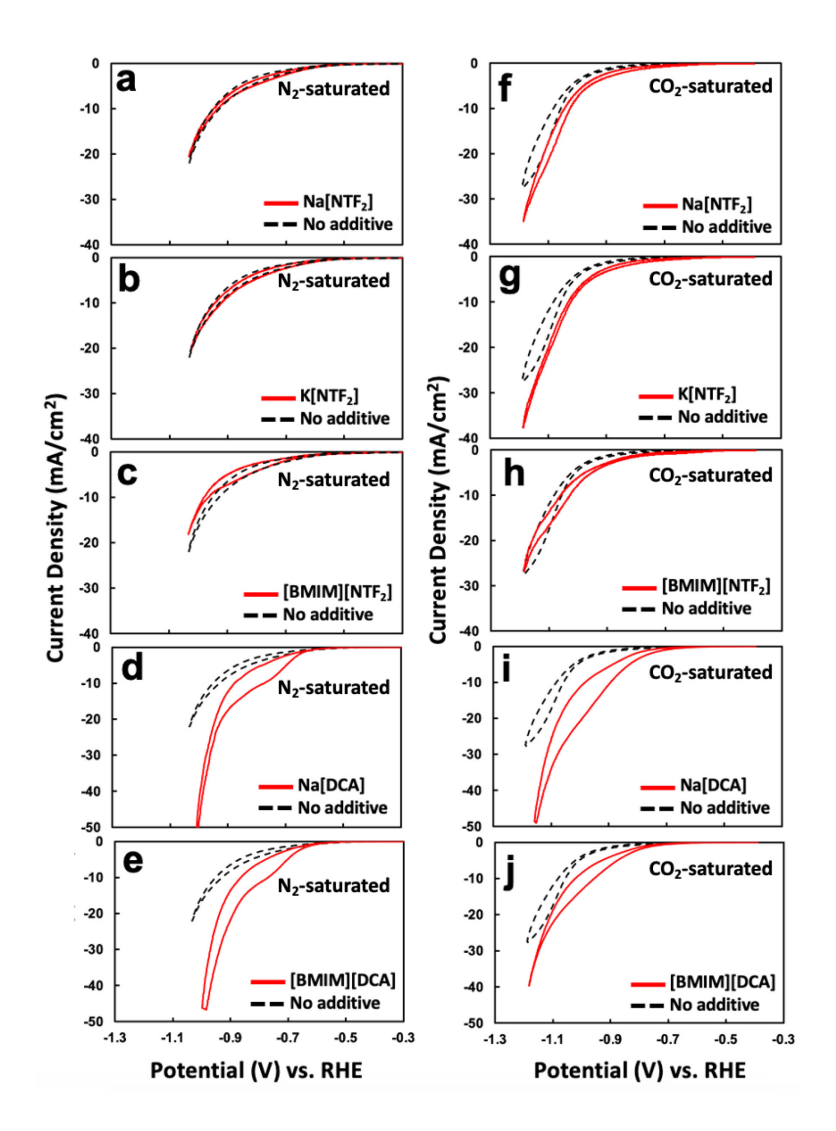


Figure 2. Comparison of the CVs for HER (a-e) and CO2ER (f-j) on Cu in electrolytes with and without 10 mM [NTF₂]⁻ and [DCA]⁻-based additives in 0.1 M KHCO₃. The electrolyte was saturated with N₂ (a-e) and CO₂ (f-j) for 30 mins before CVs measurements. Figures c, h, e, and j were reprinted with permission from Elsevier¹⁸.

In order to evaluate the product selectivity of the Cu catalyst in salt/KHCO₃ mixtures, CO2ER experiments were carried out at different potentials (-0.92 V, -1.02 V, and -1.12 V) for 30 mins on electropolished Cu electrodes. FE for the main gaseous and liquid products produced during CO2ER are shown in Figure 3a-c. It needs to be mentioned that there was also detection of methanol, n-propanol, and glycolaldehyde produced with less than 3% FE. For simplicity, only main products with higher concentrations are discussed in this article. At less negative potential (-

0.92 V), H₂, CO and formate were the main products regardless of the nature of the additives. However, at more negative potentials (-1.02 V and -1.12 V), hydrocarbons and alcohols were also produced in some electrolytes. The [DCA] electrolytes had similar product selectivity regardless of the type of cation. Both Na[DCA] and [BMIM][DCA] produced H₂ with >90% FE at -0.92 V. No C₂ products (ethylene or ethanol) were observed in Na[DCA] and [BMIM][DCA] even at the more negative potentials. Methane was the only hydrocarbon which was observed in Na[DCA] and [BMIM][DCA] at -1.12 V. In particular, FE for methane in Na[DCA] and [BMIM][DCA] were 15.5% and 6.9%, respectively. In all [NTF₂]-based electrolytes, the FE for formate was higher compared to additive-free and [DCA]—based electrolytes. Among them, [BMIM][NTF₂] had the highest FE for formate (38.7% at -0.92 V) likely due to the presence of imidazolium cation which has been previously reported to enhance the formation and stability of the CO₂• radicals on the surface and enhance CO2ER³⁰. No C₂ products were observed for [BMIM][NTF₂] and K[NTF₂] before -1.12 V, while Na[NTF₂] produced ethylene and ethanol with 19.2% FE and 6.7% FE, respectively, at -1.02 V. Therefore, the onset potential for C₂ products was more negative in [BMIM][NTF₂] and K[NTF₂] compared to additive-free electrolyte and Na[NTF₂], which has a smaller cation. This can be due to accumulation of [BMIM]⁺ and K⁺ cations at high potentials which can hinder the CO dimerization on the surface which is needed for formation of C₂ products. It has been reported that the rate-determining step (RDS) for C₂ products is C-C bond formation which occur via *CO dimerization^{52, 53}. In order to lower the CO* dimerization barrier, high coverage of *CO on catalyst surface is needed, and *CO molecules need to be close to each other⁵², ⁵³. If the *CO coverage is low or something hinders the approach of CO molecules, *CO will be converted to C₁ products^{52, 53}.

Figure 3d-f shows the partial current density for the main products in different electrolytes. The partial current density for formate increased by adding the additives in the buffer electrolytes. Both [DCA]⁻-based electrolytes had a high j_{H2} at all potentials. In particular, j_{H2} were 24.9 and 22.7 mA/cm² in [BMIM][DCA] and Na[DCA], respectively. FE% and partial current density values are also provided in Table S1 and S2.

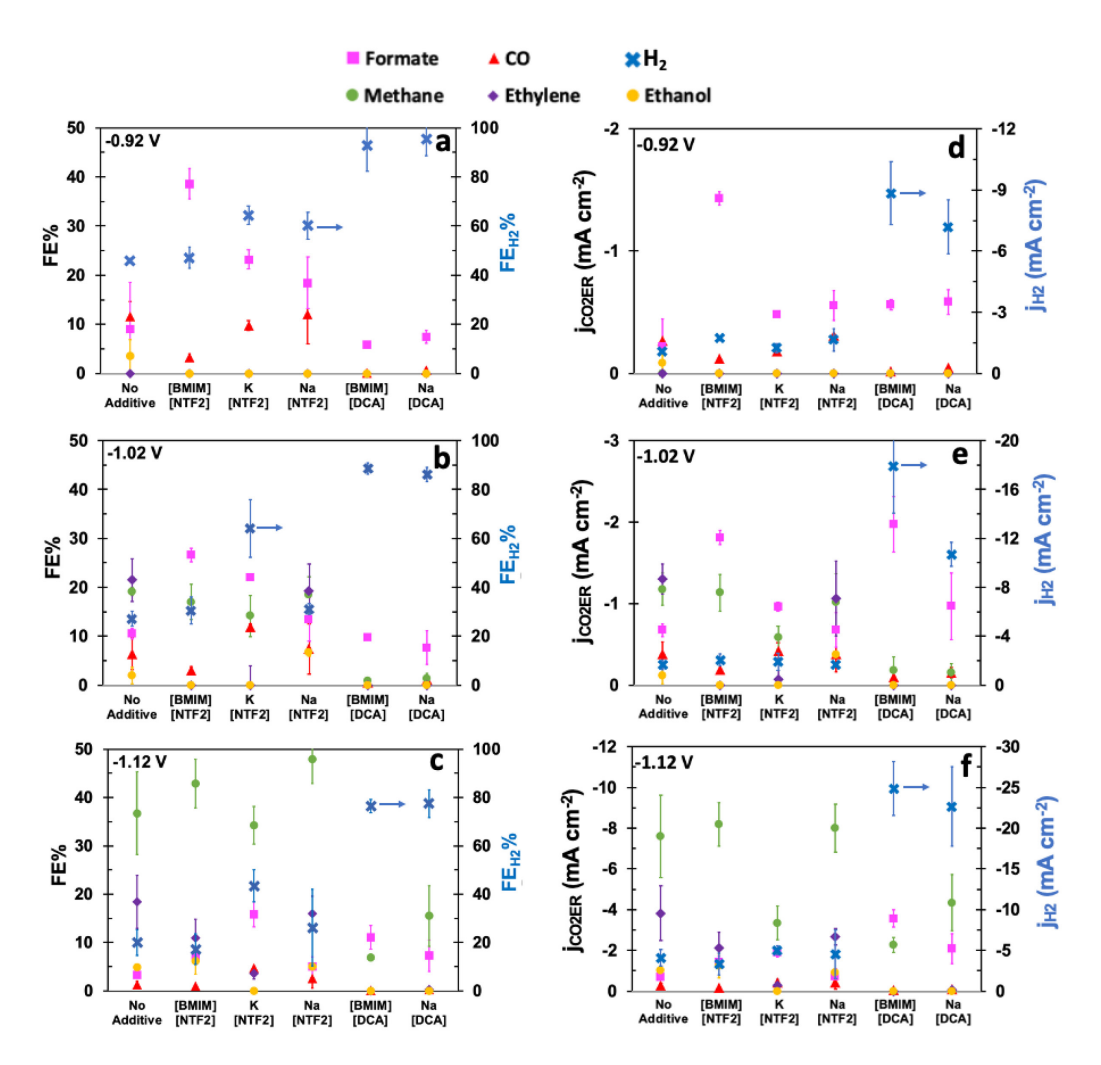


Figure 3. Faradaic efficiency (a-c) and partial current density (d-f) of the main products produced in 0.1M KHCO₃ electrolytes containing 10 mM [NTF₂]⁻ and [DCA]⁻-based additives (left and right vertical axes for each chart correspond to the products produced in CO2ER and HER reactions, respectively). Data for no additive, [BMIM][NTF₂] and [BMIM][DCA] electrolytes were adapted from our previous publication.

The effect of additive ions on the interfacial properties such as charge transfer resistance was also studied by performing EIS in the electrolytes containing [NTF₂]⁻ and [DCA]⁻ additives with different cations. Figure 4 shows the EIS results at a low (-0.82 V) and a high negative potential (-1.09 V) in CO₂-saturated electrolytes. Nyquist plots (Figure 4a-b) were fitted by using the equivalent electric circuits illustrated in Figure S1. Charge transfer and solution resistance values were then plotted in Figure 4c-d.

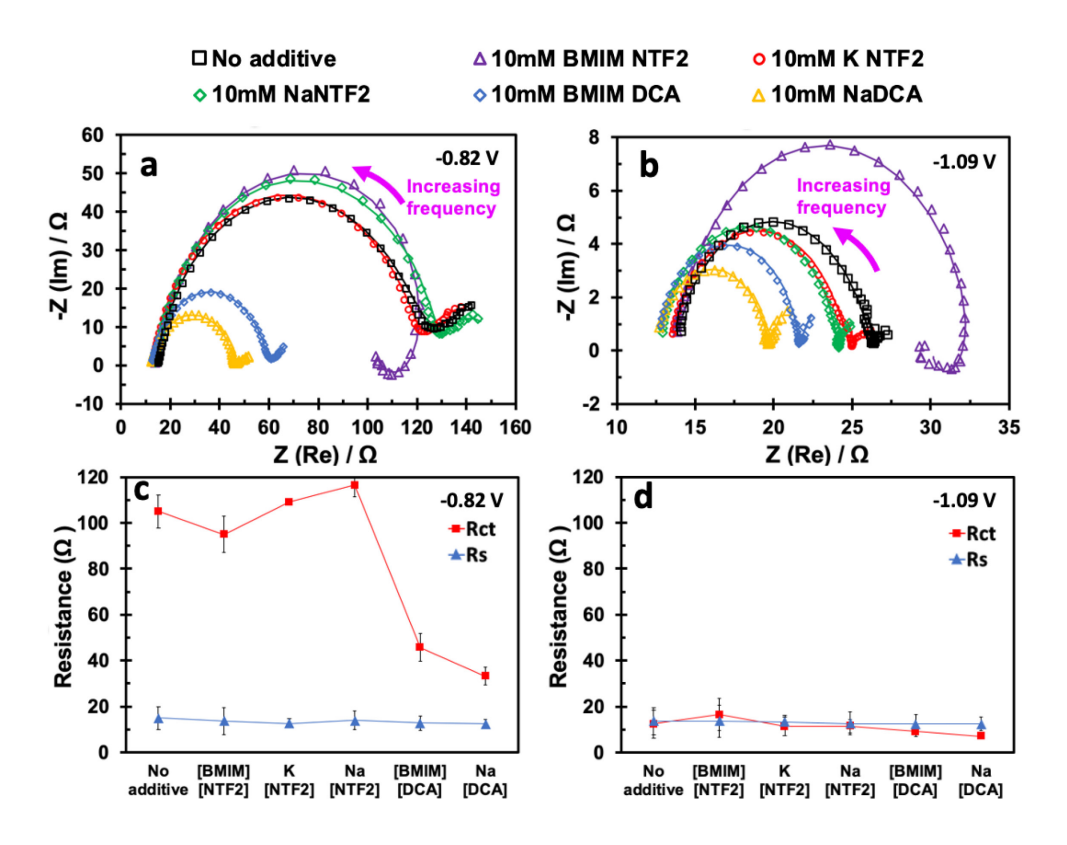


Figure 4. Nyquist plots (a-b), solution and charge transfer resistance (c-d) for the CO₂-saturated electrolytes containing 10 mM [NTF₂]⁻ and [DCA]⁻-based additives in 0.1 M KHCO₃ at -0.82 V and -1.09 V. Solid lines in a and b are the fitted curves according to the equivalent circuits in Figure S1.

According to Figure 4, the cation has a more significant impact on the interface in [NTF₂]⁻based electrolytes compared to [DCA]⁻-based electrolytes. In [NTF₂]⁻ electrolytes, the shape of the Nyquist plot in [BMIM][NTF₂] is different from that in Na[NTF₂] and K[NTF₂] at both potentials of -0.82 V and -1.09 V. The inductive loop at low frequency which had been observed for [BMIM][NTF₂] was not observed for K[NTF₂] and Na[NTF₂] at any potential (Figure 4a-b). It has been reported that the low frequency inductive loop can be associated to the adsorption/desorption of the species at the surface⁵⁴. Since the inductive loop was only observed for [BMIM][NTF₂] electrolytes, this loop can be due to the adsorption and desorption of the imidazolium on the surface and its interaction with CO₂ molecules on the surface during CO2ER. In [DCA]⁻ electrolytes, the shapes of the Nyquist plots were similar at both potentials, and no inductive loop was observed for [DCA]⁻ salts even with [BMIM]⁺ cation. This observation can

show the dominant role of the [DCA]⁻ anions at the interface compared to the cations. Figure 4c-d show the solution (R_s) and charge transfer resistance (R_{ct}) in the CO₂- saturated electrolytes containing [NTF₂]⁻- and [DCA]⁻-based additives at -0.82 V and -1.09 V. R_s depends on several factors such as electrode geometry and size, the distance between the electrodes, and also the electrolyte conductivity⁵⁵. According to Figure 4c-d, similar R_s were obtained in the electrolytes with different additives. Conductivity measurements (Figure S2) also showed that the conductivity values for all electrolytes studied here are almost similar ranging from 9600 to 11107 μS/cm.

Although the additives had a minimal influence on R_s, they had a prominent impact on the R_{ct} especially at low potentials. Electrolytes containing [DCA]⁻ salts showed a lower R_{ct} compared to the [NTF₂]⁻ salts at both potentials. In particular, R_{ct} in Na[DCA] and Na[NTF₂] are 33.5 and 116.5 ohms, respectively. Moreover, it was observed that both Na[NTF₂] and K[NTF₂] have a higher R_{ct} compared to [BMIM][NTF₂] at less negative potential (-0.82 V). However, [BMIM][NTF₂] showed a higher R_{ct} compared to inorganic salts at more negative potential (-1.09 V) likely due to the accumulation of large imidazolium cations at high overpotential which can impede diffusion of the species from bulk to the electrode surface.

In order to study the surface chemical change, XPS surface analysis was performed on the catalysts after submerging in the additive-free and additive-containing electrolytes for 4 hrs with CO₂ sparging to reach saturation with no potential applied, and also after CO2ER experiments. Carbon, oxygen, copper, and nitrogen were the only elements detected on the surface after CO2ER in electrolytes containing [NTF₂]⁻- and [DCA]⁻-based additives. The presence of the nitrogen on the surface is indicative of the strong interaction of the additives with Cu surface (Figures S7 and S8). Both [BMIM][DCA] and Na[DCA] had a higher amount of nitrogen on the surface (4.6 at.% and 10.65 at.%, respectively) compared to [NTF₂]-based additives which had less than 1% nitrogen on the surface (Figure 5a). While it may be expected that [DCA]—containing electrolytes would result in more nitrogen on the surface because there are three nitrogen atoms in a [DCA] anion and only one nitrogen atom in a [NTF₂] anion (and two nitrogen atoms in the [BMIM]⁺ cation), even after normalization to the number of nitrogen atoms in the additives (Figure 5b), a higher amount of additive was present on the copper electrode surface in the case of [BMIM][DCA] and Na[DCA] compared to [NTF₂]-based additives. The results also show that there are higher amount of N adsorbed on the surface in Na[DCA] compared to [BMIM][DCA]. This can show that [BMIM]⁺ cations and [DCA]⁻ anions compete to access the active sites on the

surface. The XPS results confirmed the strong adsorption of the [DCA]⁻-based additives on Cu surface likely due to their hydrophilic nature. Strong adsorption of the additives on the surface can suppress CO2ER by occupying sites of the surface and changing the microenvironment around the surface hindering CO₂ diffusion to the surface.

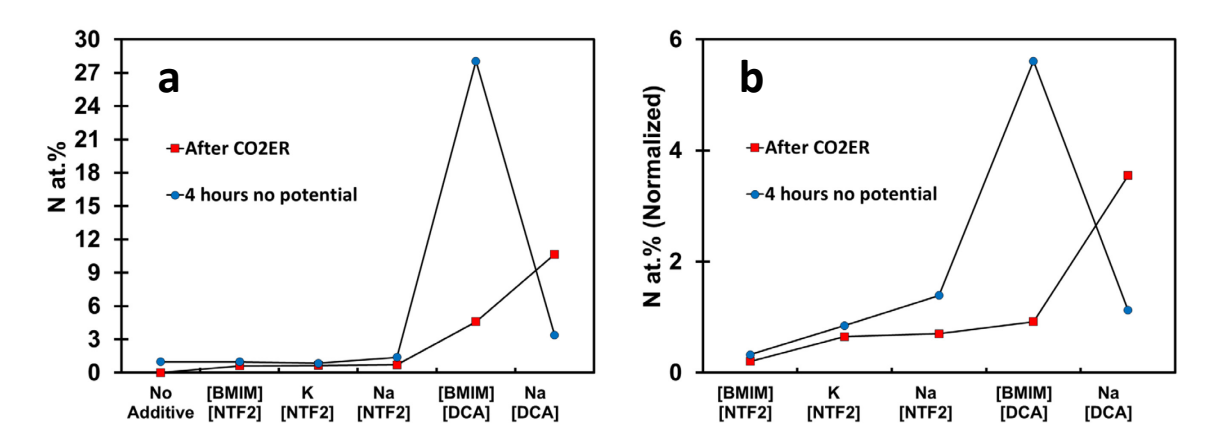


Figure 5. Atomic percentage of nitrogen detected on Cu obtained by XPS after CO2ER in electrolytes containing [NTF₂]⁻ and [DCA]⁻-based additives with different cations; a) before and b) after normalization to the number of N atoms in the salt

While it may not be expected that anions strongly adsorb to negatively charged electrodes such as the conditions in CO2ER, chemical adsorption may occur without charge attraction as well. Cu foils were submerged into electrolyte without any applied potential for four hours to simulate the duration of CO2ER experiments. The nitrogen at% for Cu foils submerged into electrolyte solutions for 4 hours with and without additives are shown in Figure 6. Similar trends are shown without an applied potential, with higher nitrogen being seen on the surface for solutions containing [DCA]⁻ anions. This shows that the [DCA]⁻ anion will adsorb to the Cu surface without an applied potential. Higher N at% is seen prior to CO2ER except in the case of the Na[DCA] additive.

In order to further study the adsorption of ions on the charged Cu surface when applying potential, EQCM paired with LSV was also performed (Figure 6). Electrolytes containing [BMIM][NTF₂], Na[NTF₂], [BMIM][DCA], and Na[DCA] additives were chosen to be used in

EQCM test. Figure 6 shows an initial mass loss during LSV for all electrolytes. This mass loss can be due to previously adsorbed ions or water molecules leaving the surface with decreasing potential. It needs to be mentioned that in EQCM, both masses of the electrode and the adjacent electrolyte layer are always detected⁵⁶. According to Figure 6, the maximum mass loss was observed for [DCA]⁻-salts especially [BMIM][DCA] probably due to the high adsorption of this IL on the surface. Therefore, with decreasing potential it is suggested that [DCA]⁻ anions leave the surface. These results confirm the XPS results which showed the strong adsorption of [DCA]⁻ based salts on the surface.

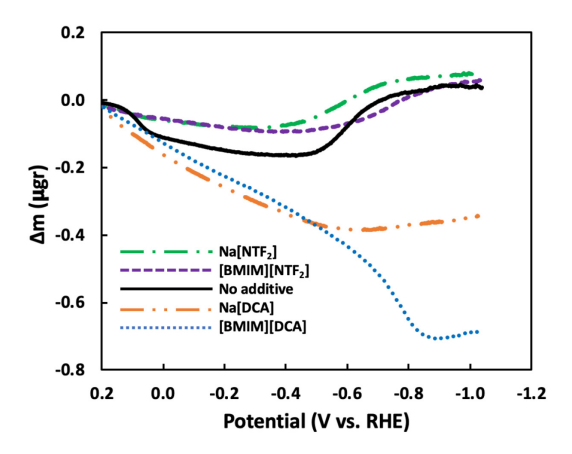


Figure 6. Mass change obtained by in-situ EQCM performed during LSV in different electrolytes.

In-situ FTIR using thin Cu films as the working electrode was done to study the CO2ER at low overpotentials with no additives and in the presence of additives. This technique has shown promise in assisting in the fundamental understanding of electrocatalytic processes and has seen significant use for the electroreduction of CO₂⁵⁷. Figure 7a-b shows the absorbance spectra without IL during CO2ER in an LSV at 1mV/s scan rate between 0 V RHE and -0.7 V RHE. All spectra are shown with a background of 64 co-averaged scans taken before electrolyte addition (i.e. air on copper surface with no potential). After addition of the 0.1 M potassium bicarbonate electrolyte, the following bands were observed: 1640 cm⁻¹ bending of the HOH molecule, 1480 cm⁻¹ for the adsorbed CO₃²⁻, 2360 cm⁻¹ from CO₂, and 3450 cm⁻¹ from OH stretch. On application of reducing potential, a decrease to the intensity of the adsorbed carbonate band was shown, likely due to electrochemical repulsion of the carbonate species. At -0.55 V RHE, a new band appeared at 2078

cm⁻¹ from linear bonding of CO to the Cu surface with a 2 cm⁻¹ downward shift when the potential was further decreased to -0.70 V. These bands were consistent with similar works of CO2ER on Cu films^{47, 58}. More negative potentials than -0.70 V were not able to be studied due to bubble formation on the Cu film and delamination of the Cu film.

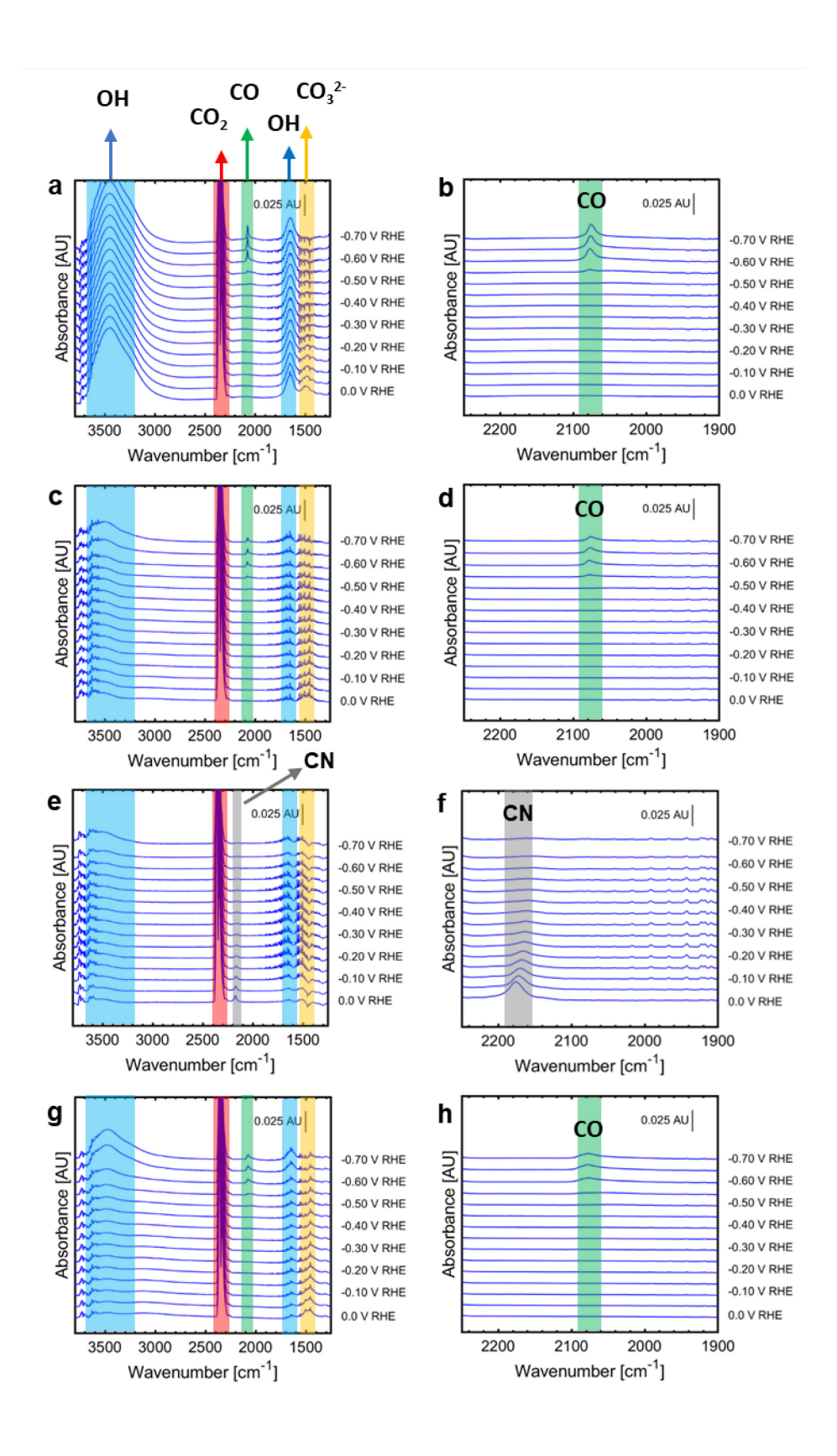


Figure 7. FTIR spectra during CO2ER over a Cu film deposited onto an ATR crystal. Solution of CO₂ saturated 0.1M KHCO₃ with (a-b) no additive, (c-d) 10mM [BMIM][NTF₂], (e-f) [BMIM][DCA], (g-h) K[NTF₂]. LSV from 0.0 V to -0.7 V at a scan rate of 1 mV/s. Spectra are 16 co-averaged scans at a resolution of 4 cm⁻¹.

The addition of any IL tested in this analysis had the impact of reducing the intensity of the HOH bending, adsorbed CO₃²⁻, and OH stretching bands (Figure 7c-h). This was likely a result of displacement of water and carbonate from the surface of the Cu at the ATR crystal. The FTIR spectra for CO2ER in the presence of 10mM [BMIM][NTF₂] is shown in Figure 7c-d. Similar to the spectra obtained with no IL, the appearance of the CO band occurred at -0.55 V RHE, however HOH bending and OH stretching from the water molecules were significantly lower in intensity compared to the IL free solution.

Figure 7e-f shows the obtained FTIR spectra for CO2ER in the presence of 10 mM [BMIM][DCA]. [DCA]⁻ anions showed an IR band at 2180 cm⁻¹ corresponding to the symmetric CN triple bond stretch⁵⁹. This shows that the [DCA]⁻ anion will strongly adsorb to the Cu surface without an applied potential rapidly. On application of a negative applied potential, the CN triple bond band of the [DCA]⁻ anion decreased in magnitude due to the electrochemical repulsion of the anion from the negatively-charged surface. Dissimilar to other electrolytes tested, no CO band appeared during LSV from 0 V to -0.7 V, further supporting the CO2ER FE% and partial current density observations that CO2ER was minimized when [BMIM][DCA] was present.

Figure 7g-h shows the FTIR spectra in the presence of 10 mM K[NTF₂]. Similar trends were seen compared to [BMIM][NTF₂], however a more rapid increase of the OH stretch and HOH bending with decreasing applied potential could suggest that diffusion of the water molecules to the surface can occur more rapidly due to less bulky ions at the Cu surface and hydration around the K⁺ cation.

The onset of the CO band, at approximately -0.55 V vs RHE, corresponded with the onset of mass increase in the EQCM experiments. This suggests that the mass increase is due to CO adsorption. Additionally, a decrease in the mass of the electrode determined by EQCM of the [DCA]⁻ anion containing electrolyte with decreasing potential could be due to the repulsion of [DCA]⁻ anion from the surface with increasing negative potential. While the FTIR spectra was limited to -0.70 V RHE, due to delamination and bubbling at more negative potentials, EQCM results showed an increase to the mass of electrode with [DCA]⁻ containing electrolytes at more

negative potentials then other electrolytes which could suggest a later onset of CO adsorption to the surface, supported by the lack of a CO band between 0 and -0.70 V RHE in the FTIR spectra.

The onset potential for solutions not containing [DCA]⁻, with CO₂ sparging, also appeared at -0.55 V, which can be seen in Figure 2-f,g,h. This suggests that CO₂ reduction could occur at a small rate at -0.55 V. With either the [BMIM][DCA] or Na[DCA] additive at 10mM, the onset potential was shifted to a more negative potential around -0.65 V. While the onset potential appears at -0.65 V, there was no corresponding CO band appearing during FTIR spectra at -0.65 V which suggested the onset could be due to HER instead of a CO₂ reduction through the CO intermediate.

Furthermore, EQCM showed an increase in mass of the Cu surface in electrolytes not containing [DCA]⁻ around -0.55 V as well, suggesting that the mass increase was due to bound CO molecules. For Na[DCA] electrolyte, while the mass did not further decrease beyond -0.5 V it did not increase suggesting no CO adsorption. The same was seen on [BMIM][DCA], although requiring a more negative potential to stop the mass loss. Figure 3 showed that the [DCA]⁻- containing electrolytes had a much lower Faradaic efficiency to CO at each potential tested for product analysis, with a higher Faradaic efficiency of HER. This is in agreement with the FTIR results showing no CO band within the potential range tested. Due to limitations of the Cu film delamination at more negative potentials, FTIR analysis could not be completed at more negative potentials to provide insights into other products.

While we show that [DCA]⁻ anions are desorbed, we see that they have an impact on the selectivity of products at more negative potentials. This could be due to the presence of anions in the vicinity of the surface which influence the transport of molecules like H₂O and CO₂ in the double layer, rather than directly at the catalyst surface. Therefore, although [DCA]⁻ is not directly adsorbed to the catalyst surface when applying negative potential, they are still in the vicinity of the catalyst probably next to the adsorbed cations, and impact the transport of the species in the boundary layer. The CO₂ affinity and hydrophobicity of the anion likely plays a key role in the influence of transport. We showed that anions with high hydrophilicity and low CO₂ affinity like [DCA]⁻ increased the FE_{H2}, while [NTF₂]⁻ anions which have a high CO₂ affinity and high hydrophobicity increased the FE_{formate}.

3.2. Effect of Additive Ions on the Local Environment of Catalyst-Electrolyte Interface

COMSOL Multiphysics was used to model CO2ER in the vicinity of the cathode and calculate the cathode-electrolyte interfacial properties such as local pH and species concentrations. Figure 8a shows the pH profile in the boundary layer around the cathode. OH⁻ concentration profile has been also provided in Figure S10 in the Supporting Information. According to Figure 8a, all electrolytes have a higher pH at the catalyst surface (x=0) compared to the bulk pH (x=100 μm). This pH rise from bulk toward cathode surface is due to formation of OH⁻ ions in CO2ER and HER reactions (Rxn. S5 to Rxn. S10). Results show that [DCA]-based electrolytes have a higher local pH compared to [NTF₂]⁻-based and additive free electrolytes. A correlation between local pH and HER current density (obtained from Figure 3) was also observed (Figure 8b). A higher HER activity was observed when local pH increases. Since HER reaction is pH-independent, it would not be expected to see any pH dependency for HER activity. However, our study and other studies^{60, 61} showed that there is a relationship between the pH and HER activity. Although the reason for this observation is not fully understood yet, some researchers believe that the enhanced HER activity in high local pH can be attributed to the enhanced hydrogen binding energy which is needed for high HER rate^{60, 62}. The CO₂ concentration profile in the boundary layer was also calculated. According to Figure 8c, a drop in CO₂ concentration from bulk to interface was observed for all electrolytes. Since CO2 is a reactant in CO2ER (Rxn. S5 to Rxn. S9) and also in buffer chemical reactions (Rxn. S2 and Rxn. S3), CO₂ concentration at interface is determined by both CO2ER current density on the electrode surface and the buffer reactions in the vicinity of the electrode. Figure 8d shows that the [NTF₂] additives, which have a higher CO2ER activity, have a lower CO₂ concentration. However, the same trend was not observed for [DCA]⁻ additives. Although [DCA] additives have a low CO2ER current, the CO₂ concentrations are low at the interface. This observation is due to the high local pH which was observed for [DCA]-based electrolytes. Increased local pH further lowers the CO₂ concentration at the interface due to the reaction of CO₂ with OH⁻ ions which leads to the formation of bicarbonate and carbonate (Rxn. S2 and Rxn. S3). Figure 8e shows that the CO₂ concentration at interface is inversely proportional to the local pH. For example, [BMIM][DCA] which has the maximum local pH (10.22), it also has the lowest CO₂ concentration at the surface (13.6 mol/m³). Among [NTF₂]⁻ additives, BMIM[NTF₂] has a higher pH and lower CO₂ concentration due to its high CO2ER activity compared to Na[NTF₂] and K[NTF₂]. It needs to be mentioned that the difference between local pH and bulk pH for additive-free electrolyte is lower compared to additive-containing electrolytes

due to the lower activity of the catalyst in additive-free electrolyte (Figure 8a). Due to the lower local pH and also lower CO2ER activity, the interfacial CO₂ concentration in additive-free electrolyte has the highest value (Figure 8d-e). Figure 9a-b display the bicarbonate and carbonate concentration profiles in the boundary layer. Since the reaction rate constant for bicarbonate formation in Rxn. S2 is much smaller than that for carbonate formation in Rxn. S3 bicarbonates are rapidly converted to carbonates at high pH. Therefore, [BMIM][DCA] has the lowest HCO₃⁻ (Figure 9a) and the highest CO₃²⁻ (Figure 9b) concentrations at the surface.

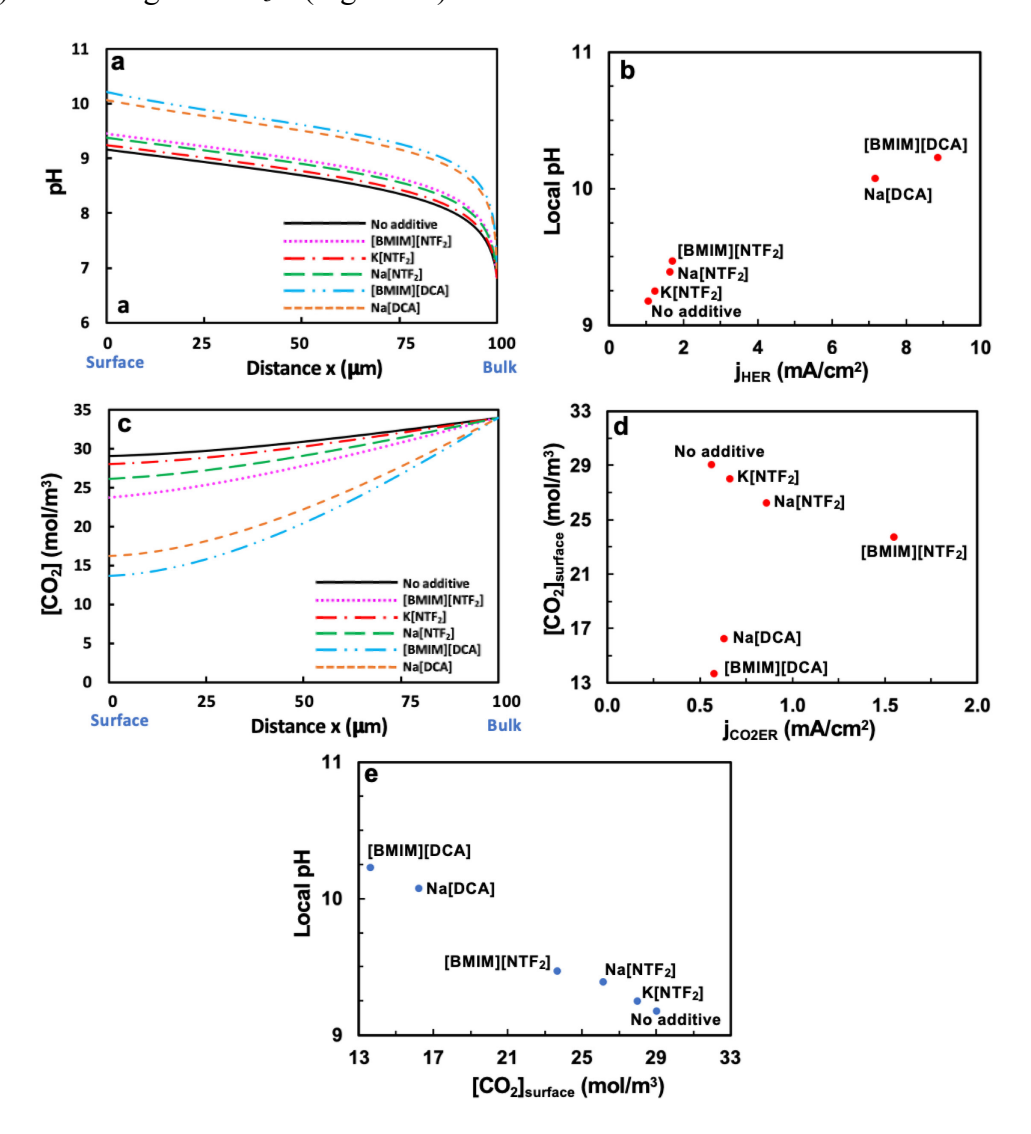


Figure 8. COMSOL calculations for a) pH profile in the boundary layer, b) correlation of local pH and partial current density for hydrogen evolution reaction (j_{HER}), c) CO₂ concentration profile in the boundary layer, d) j_{CO2ER} and interfacial CO₂ concentration ([CO₂]_{surface}) e) correlation of local pH and interfacial CO₂ concentration ([CO₂]_{surface}) in CO2ER at -0.92 V vs.

RHE in additive-free electrolyte (0.1 M KHCO₃) and in electrolytes containing 10 mM [NTF₂]⁻-and [DCA]⁻-based additives.

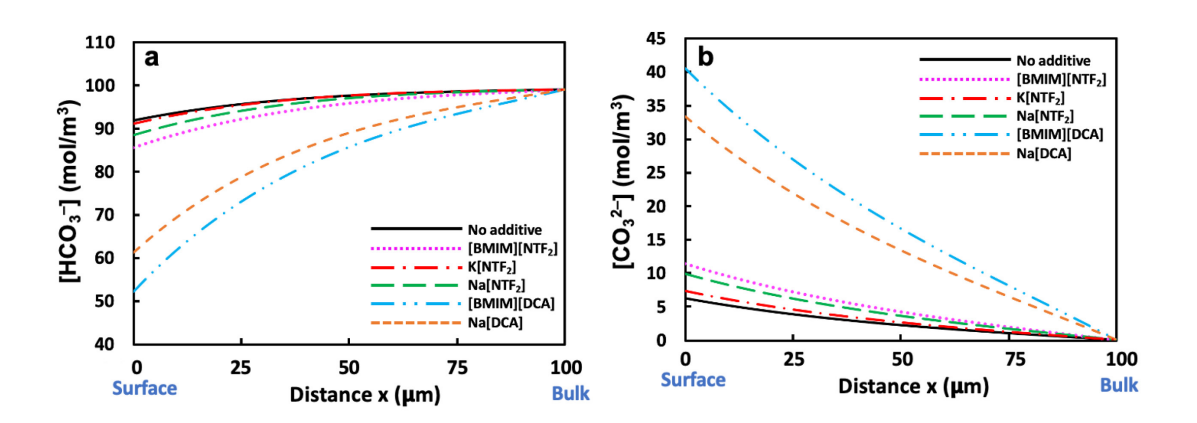


Figure 9. COMSOL calculations for: a) HCO_3^- concentration profile, and b) CO_3^{2-} concentration profile in the boundary layer in CO2ER at -0.92 V vs. RHE in additive-free electrolyte (0.1 M KHCO₃) and in electrolytes containing 10 mM [NTF₂]⁻- and [DCA]⁻-based additives.

4. CONCLUSION

Herein, we observed that electrolyte-electrode interfacial environment significantly impacts the product selectivity and catalytic activity in CO₂ electroreduction and in the competing hydrogen evolution on Cu. It was also found that the interface can be modified by using ionic additives at concentrations even as low as 10 mM. We showed that both anion and cation are important in CO2ER, with the anion having a stronger influence on the reactions. It was found that the hydrophobicity and CO₂ affinity of the additive anion plays a key role in the local environment at the surface and CO2ER activity. All [NTF₂]⁻-based additives increased the FE for formate compared to the additive-free electrolyte (9% FE) due to the high CO₂ affinity and hydrophobicity of the [NTF₂]⁻-based additives. Among [NTF₂]⁻-based additives, [BMIM][NTF₂] had a higher FE for formate (38.7%) compared to K[NTF₂] (23.2%) and Na[NTF₂] (18.5%) at -0.92 V likely due to the presence of imidazolium cation which can further stabilize the intermediates on the surface and enhance CO2ER. However, the FE for C₂ products (ethylene and ethanol) at high negative potentials were lower for [BMIM][NTF₂] and K[NTF₂] compared to the additive-free and Na[NTF₂] electrolytes. This observation can be due to the presence of large [BMIM]⁺ and hydrated

K⁺ cations on the surface and inhibiting the *CO dimerization which is needed for the formation

of C₂ products. Electrolytes containing [DCA]-based additives had a very high HER activity

(>90% FE_{H2}) and low CO2ER activity regardless of the cation nature. This observation is

attributed to the presence of [BMIM][DCA] in the vicinity of the catalyst which impacts the

microenvironment around the catalyst. Results showed that [DCA] anions have a high affinity to

adsorb on Cu catalysts when no external potential is applied. Although it was shown that [DCA]

anions desorb from the surface at negative potentials, we believe that [DCA] anions still remain

in the vicinity of the electrode, next to the adsorbed cations. The presence of [DCA] anions in the

boundary layer impacts the transport of H₂O and CO₂ and alter the product selectivity. COMSOL

calculations showed that that the local pH is directly proportional to the H₂ evolution activity.

Also, hydrophilic salts such as [DCA]-based salts were found to have a more alkaline local pH

which leads to a lower CO₂ concentration in the vicinity of the catalyst.

Supporting Information

Equivalent circuit for EIS, conductivity values of electrolytes, EQCM setup, information for

building COMSOL simulation, XPS with and without externally applied potential, Faradaic

efficiency and current density data for different potential.

Acknowledgments

The authors would like to thank the financial support for the CO2ER work from the National

Science Foundation Award CBET-1935957. The development of the FTIR SEIRAS technique in

our laboratory was supported by the U.S. Department of Energy, Office of Science, Office of Basic

Energy Sciences, Catalysis Science program, under Award DE-SC0019134 The authors also

acknowledge Surface Science Core Facility and Biomolecular NMR Facility for XPS and NMR

analysis, respectively, as well as the Nanoscience Initiative in Advanced Science Research Center

(ASRC) at the Graduate Center in CUNY. The authors thank Professor Bingjun Xu and Dr. Arnav

Malkani for sharing and teaching the process to coat Cu onto Si ATR crystals for in-situ FTIR.

The help of Dr. James Aramini and Dr. Denize Favaro in NMR experiments is also appreciated.

ORCID

Samaneh Sharifi Golru: 0000-0002-0136-7555

24

Andrew S. May: 0000-0001-7780-2907

Elizabeth J. Biddinger: 0000-0003-3616-1108

References

- (1) Global monitoring laboratory-carbon cycle greenhouse gases; Global Monitoring Laboratory . https://gml.noaa.gov/ccgg/trends/global.html, 2021.
- (2) Sánchez, O. G.; Birdja, Y. Y.; Bulut, M.; Vaes, J.; Breugelmans, T.; Pant, D. Recent advances in industrial CO₂ electroreduction. *Current Opinion in Green and Sustainable Chemistry* 2019, *16*, 47-56. DOI: https://doi.org/10.1016/j.cogsc.2019.01.005.
- (3) Hori, Y.; Murata, A.; Takahashi, R. Formation of hydrocarbons in the electrochemical reduction of carbon dioxide at a copper electrode in aqueous solution. *J. Chem. Soc., Faraday Trans. 1* 1989, 85 (8), 2309-2326, 10.1039/F19898502309. DOI: 10.1039/F19898502309.
- (4) Hori, Y.; Wakebe, H.; Tsukamoto, T.; Koga, O. Electrocatalytic process of CO selectivity in electrochemical reduction of CO₂ at metal electrodes in aqueous media. *Electrochim. Acta* 1994, 39 (11–12), 1833-1839. DOI: http://dx.doi.org/10.1016/0013-4686(94)85172-7.
- (5) Zhang, L.; Zhao, Z.-J.; Gong, J. Nanostructured materials for heterogeneous electrocatalytic CO₂ reduction and their related reaction mechanisms. *Angew. Chem., Int. Ed.* 2017, *56* (38), 11326-11353. DOI: 10.1002/anie.201612214 (accessed 2019/04/09).
- (6) Liu, H. L.; Zhu, Y. T.; Ma, J. M.; Zhang, Z. C.; Hu, W. P. Recent advances in atomic-level engineering of nanostructured catalysts for electrochemical CO₂ reduction. *Advanced Functional Materials* 2020, *30* (17). DOI: 10.1002/adfm.201910534.
- (7) Whipple, D. T.; Finke, E. C.; Kenis, P. J. A. Microfluidic reactor for the electrochemical reduction of carbon dioxide: The effect of pH. *Electrochemical and Solid-State Letters* 2010, *13* (9), B109. DOI: 10.1149/1.3456590.
- (8) Weekes, D. M.; Salvatore, D. A.; Reyes, A.; Huang, A.; Berlinguette, C. P. Electrolytic CO₂ reduction in a flow cell. *Accounts of Chemical Research* 2018, *51* (4), 910-918. DOI: 10.1021/acs.accounts.8b00010.
- (9) Karaiskakis, A. N.; Sharifi Golru, S.; Biddinger, E. J. Effect of electrode geometry on selectivity and activity in CO₂ electroreduction. *Ind. Eng. Chem. Res.* 2019, *58*, 22506-22515.
- (10) Varela, A. S.; Ju, W.; Reier, T.; Strasser, P. Tuning the catalytic activity and selectivity of Cu for CO₂ electroreduction in the presence of halides. *ACS Catal.* 2016, *6* (4), 2136-2144. DOI: 10.1021/acscatal.5b02550.

- (11) Verma, S.; Lu, X.; Ma, S.; Masel, R. I.; Kenis, P. J. A. The effect of electrolyte composition on the electroreduction of CO₂ to CO on Ag based gas diffusion electrodes. *Phys. Chem. Chem. Phys.* 2016, *18* (10), 7075-7084, 10.1039/C5CP05665A. DOI: 10.1039/C5CP05665A.
- (12) Singh, M. R.; Kwon, Y.; Lum, Y.; Ager, J. W.; Bell, A. T. Hydrolysis of electrolyte cations enhances the electrochemical reduction of CO₂ over Ag and Cu. *J. Am. Chem. Soc.* 2016, *138* (39), 13006-13012. DOI: 10.1021/jacs.6b07612.
- (13) Qiao, J.; Liu, Y.; Hong, F.; Zhang, J. A review of catalysts for the electroreduction of carbon dioxide to produce low-carbon fuels. *Chem. Soc. Rev.* 2014, *43* (2), 631-675, 10.1039/C3CS60323G. DOI: 10.1039/C3CS60323G.
- (14) Quan, F.; Xiong, M.; Jia, F.; Zhang, L. Efficient electroreduction of CO₂ on bulk silver electrode in aqueous solution via the inhibition of hydrogen evolution. *Appl. Surf. Sci.* 2017, *399*, 48-54. DOI: https://doi.org/10.1016/j.apsusc.2016.12.069.
- (15) Long, C.; Li, X.; Guo, J.; Shi, Y.; Liu, S.; Tang, Z. Electrochemical reduction of CO₂ over heterogeneous catalysts in aqueous solution: Recent progress and perspectives. *Small Methods* 2019, *3* (3), 1800369. DOI: 10.1002/smtd.201800369.
- (16) Nitopi, S.; Bertheussen, E.; Scott, S. B.; Liu, X.; Engstfeld, A. K.; Horch, S.; Seger, B.; Stephens, I. E. L.; Chan, K.; Hahn, C.; Nørskov, J. K.; Jaramillo, T. F.; Chorkendorff, I. Progress and perspectives of electrochemical CO₂ reduction on copper in aqueous electrolyte. *Chem. Rev.* 2019, 119 (12), 7610-7672. DOI: 10.1021/acs.chemrev.8b00705.
- (17) Sharifi Golru, S.; Biddinger, E. J. Effect of additives in aqueous electrolytes on CO₂ electroreduction. *Chem. Eng. J.* 2022, *428*, 131303. DOI: https://doi.org/10.1016/j.cej.2021.131303.
- (18) Sharifi Golru, S.; Biddinger, E. J. Effect of anion in diluted imidazolium-based ionic liquid/buffer electrolytes for CO₂ electroreduction on copper. *Electrochim. Acta* 2020, *375*, 136787. DOI: https://doi.org/10.1016/j.electacta.2020.136787.
- (19) Feaster, J. T.; Jongerius, A. L.; Liu, X. Y.; Urushihara, M.; Nitopi, S. A.; Hahn, C.; Chan, K.; Norskov, J. K.; Jaramillo, T. F. Understanding the influence of EMIM CI on the suppression of the hydrogen evolution reaction on transition metal electrodes. *Langmuir* 2017, *33* (37), 9464-9471. DOI: 10.1021/acs.langmuir.7b01170.

- (20) Hailu, A.; Shaw, S. K. Efficient electrocatalytic reduction of carbon dioxide in 1-ethyl-3-methylimidazolium trifluoromethanesulfonate and water mixtures. *Energy Fuels* 2018, *32* (12), 12695-12702. DOI: 10.1021/acs.energyfuels.8b02750.
- (21) Zarandi, R. F.; Rezaei, B.; Ghaziaskar, H. S.; Ensafi, A. A. Electrochemical reduction of CO₂ to ethanol using copper nanofoam electrode and 1-butyl-3-methyl-imidazolium bromide as the homogeneous co-catalyst. *Journal of Environmental Chemical Engineering* 2019, 7 (3), 103141. DOI: https://doi.org/10.1016/j.jece.2019.103141.
- (22) Rudnev, A. V.; Kiran, K.; Cedeño López, A.; Dutta, A.; Gjuroski, I.; Furrer, J.; Broekmann, P. Enhanced electrocatalytic CO formation from CO₂ on nanostructured silver foam electrodes in ionic liquid/water mixtures. *Electrochim. Acta* 2019, *306*, 245-253. DOI: https://doi.org/10.1016/j.electacta.2019.03.102.
- (23) Zhou, F.; Liu, S.; Yang, B.; Wang, P.; Alshammari, A. S.; Deng, Y. Highly selective electrocatalytic reduction of carbon dioxide to carbon monoxide on silver electrode with aqueous ionic liquids. *Electrochem. Commun.* 2014, *46*, 103-106. DOI: https://doi.org/10.1016/j.elecom.2014.06.023.
- (24) Huan, T. N.; Simon, P.; Rousse, G.; Génois, I.; Artero, V.; Fontecave, M. Porous dendritic copper: an electrocatalyst for highly selective CO₂ reduction to formate in water/ionic liquid electrolyte. *Chemical Science* 2017, 8 (1), 742-747, 10.1039/C6SC03194C. DOI: 10.1039/C6SC03194C.
- **(25)** Han, Z.; Kortlever, R.; Chen, H.-Y.; Peters, J. C.; Agapie, T. CO₂ reduction selective for C_{≥2} products on polycrystalline copper with N-substituted pyridinium additives. *ACS Central Science* 2017, *3* (8), 853-859. DOI: 10.1021/acscentsci.7b00180.
- (26) Dufek, E. J.; Lister, T. E.; McIlwain, M. E. Influence of electrolytes and membranes on cell operation for syn-gas production. *Electrochemical and Solid-State Letters* 2012, *15* (4), B48. DOI: 10.1149/2.010204esl.
- (27) Lv, J.-J.; Jouny, M.; Luc, W.; Zhu, W.; Zhu, J.-J.; Jiao, F. A highly porous copper electrocatalyst for carbon dioxide reduction. *Advanced Materials* 2018, *30* (49), 1803111, https://doi.org/10.1002/adma.201803111. DOI: https://doi.org/10.1002/adma.201803111 (accessed 2021/01/25).
- (28) Thevenon, A.; Rosas-Hernández, A.; Peters, J. C.; Agapie, T. In-situ nanostructuring and stabilization of polycrystalline copper by an organic salt additive promotes electrocatalytic CO₂

- reduction to ethylene. *Angew. Chem., Int. Ed.* 2019, *58* (47), 16952-16958. DOI: 10.1002/anie.201907935 (accessed 2020/09/18).
- (29) Banerjee, S.; Han, X.; Thoi, V. S. Modulating the electrode-electrolyte interface with cationic surfactants in carbon dioxide reduction. *ACS Catal.* 2019, *9* (6), 5631-5637. DOI: 10.1021/acscatal.9b00449.
- (30) Rosen, B. A.; Salehi-Khojin, A.; Thorson, M. R.; Zhu, W.; Whipple, D. T.; Kenis, P. J. A.; Masel, R. I. Ionic liquid-mediated selective conversion of CO₂ to CO at low overpotentials. *Science* 2011, *334* (6056), 643-644, Article. DOI: 10.1126/science.1209786.
- (31) Huang, Y.; Ong, C. W.; Yeo, B. S. Effects of electrolyte anions on the reduction of carbon dioxide to ethylene and ethanol on copper (100) and (111) surfaces. *Chemsuschem* 2018, *11* (18), 3299-3306. DOI: 10.1002/cssc.201801078.
- (32) Gao, D. F.; Sohoken, F.; Roldan Cuenya, B. Improved CO₂ electroreduction performance on plasma-activated Cu catalysts via electrolyte design: Halide effect. *ACS Catal.* 2017, 7 (8), 5112-5120. DOI: 10.1021/acscatal.7b01416.
- (33) Salehi-Khojin, A.; Jhong, H.-R. M.; Rosen, B. A.; Zhu, W.; Ma, S.; Kenis, P. J. A.; Masel, R. I. Nanoparticle silver catalysts that Show enhanced activity for carbon dioxide electrolysis. *J. Phys. Chem. C* 2013, *117* (4), 1627-1632. DOI: 10.1021/jp310509z.
- (34) Rudnev, A. V.; Fu, Y. C.; Gjuroski, I.; Stricker, F.; Furrer, J.; Kovacs, N.; Vesztergom, S.; Broekmann, P. Transport matters: Boosting CO₂ electroreduction in mixtures of BMIm BF₄ /water by enhanced diffusion. *Chemphyschem* 2017, *18* (22), 3153-3162. DOI: 10.1002/cphc.201700737.
- (35) Zhang, X.; Zhao, Y.; Hu, S.; Gliege, M. E.; Liu, Y.; Liu, R.; Scudiero, L.; Hu, Y.; Ha, S. Electrochemical reduction of carbon dioxide to formic acid in ionic liquid [Emim][N(CN)₂]/water system. *Electrochim. Acta* 2017, *247*, 281-287. DOI: https://doi.org/10.1016/j.electacta.2017.06.112.
- (36) Dong, Q.; Zhang, X. Z.; He, D.; Lang, C. C.; Wang, D. W. Role of H₂O in CO₂ electrochemical reduction as studied in a water-in-salt system. *ACS Central Science* 2019, *5* (8), 1461-1467. DOI: 10.1021/acscentsci.9b00519.
- (37) Hong, S.; Lee, S.; Kim, S.; Lee, J. K.; Lee, J. Anion dependent CO/H₂ production ratio from CO₂ reduction on Au electro-catalyst. *Catal. Today* 2017, *295*, 82-88. DOI: 10.1016/j.cattod.2017.05.063.

- (38) Neubauer, S. S.; Krause, R. K.; Schmid, B.; Guldi, D. M.; Schmid, G. Overpotentials and faraday efficiencies in CO₂ electrocatalysis—the impact of 1-ethyl-3-methylimidazolium trifluoromethanesulfonate. *Advanced Energy Materials* 2016, 6 (9), 1502231. DOI: 10.1002/aenm.201502231.
- (39) Bockris, J. O. M.; Conway, B. E.; Yeager, E. Comprehensive treatise of electrochemistry: Vol.1: The double layer; Plenum Press, 1980.
- (40) Singh, M. R.; Goodpaster, J. D.; Weber, A. Z.; Head-Gordon, M.; Bell, A. T. Mechanistic insights into electrochemical reduction of CO₂ over Ag using density functional theory and transport models. *Proc. Natl. Acad. Sci. U. S. A.* 2017, *114* (42), E8812-E8821. (accessed 2021/06/16/).JSTOR.
- (41) Aydin, F.; Zhan, C.; Ritt, C.; Epsztein, R.; Elimelech, M.; Schwegler, E.; Pham, T. A. Similarities and differences between potassium and ammonium ions in liquid water: a first-principles study. *Phys. Chem. Chem. Phys.* 2020, *22* (4), 2540-2548. DOI: 10.1039/c9cp06163k.
- (42) Hribar, B.; Southall, N. T.; Vlachy, V.; Dill, K. A. How ions affect the structure of water. *J. Am. Chem. Soc.* 2002, *124* (41), 12302-12311. DOI: 10.1021/ja026014h.
- (43) Niu, D.; Wang, H.; Li, H.; Wu, Z.; Zhang, X. Roles of ion pairing on electroreduction of carbon dioxide based on imidazolium-based salts. *Electrochim. Acta* 2015, *158*, 138-142. DOI: https://doi.org/10.1016/j.electacta.2015.01.096.
- (44) Kemna, A.; Rey, N. G.; Braunschweig, B. Mechanistic insights on CO₂ reduction reactions at platinum/ BMIM BF₄ interfaces from in operando spectroscopy. *ACS Catal.* 2019, *9* (7), 6284-6292. DOI: 10.1021/acscatal.9b01033.
- (45) Wang, Y. Q.; Hatakeyama, M.; Ogata, K.; Wakabayashi, M.; Jin, F. M.; Nakamura, S. Activation of CO₂ by ionic liquid EMIM-BF₄ in the electrochemical system: a theoretical study. *Phys. Chem. Chem. Phys.* 2015, *17* (36), 23521-23531, Article. DOI: 10.1039/c5cp02008e.
- (46) Cadena, C.; Anthony, J. L.; Shah, J. K.; Morrow, T. I.; Brennecke, J. F.; Maginn, E. J. Why is CO₂ so soluble in imidazolium-based ionic liquids? *J. Am. Chem. Soc.* 2004, *126* (16), 5300-5308. DOI: 10.1021/ja039615x (accessed 2014/02/09).
- (47) Gunathunge, C. M.; Li, X.; Li, J.; Hicks, R. P.; Ovalle, V. J.; Waegele, M. M. Spectroscopic observation of reversible surface reconstruction of copper electrodes under CO₂ reduction. *J. Phys. Chem. C* 2017, *121* (22), 12337-12344. DOI: 10.1021/acs.jpcc.7b03910.

- (48) Hashiba, H.; Weng, L.-C.; Chen, Y.; Sato, H. K.; Yotsuhashi, S.; Xiang, C.; Weber, A. Z. Effects of electrolyte buffer capacity on surface reactant species and the reaction rate of CO₂ in electrochemical CO₂ reduction. *J. Phys. Chem. C* 2018, *122* (7), 3719-3726. DOI: 10.1021/acs.jpcc.7b11316.
- (49) Banerjee, S.; Zhang, Z. Q.; Hall, A. S.; Thoi, V. S. Surfactant perturbation of cation interactions at the electrode-electrolyte interface in carbon dioxide reduction. *ACS Catal.* 2020, *10* (17), 9907-9914. DOI: 10.1021/acscatal.0c02387.
- (50) Li, J. Y.; Li, X.; Gunathunge, C. M.; Waegele, M. M. Hydrogen bonding steers the product selectivity of electrocatalytic CO reduction. *Proc. Natl. Acad. Sci. U. S. A.* 2019, *116* (19), 9220-9229. DOI: 10.1073/pnas.1900761116.
- (51) Ge, W. X.; Chen, Y. X.; Fan, Y.; Zhu, Y. H.; Liu, H. L.; Song, L.; Liu, Z.; Lian, C.; Jiang, H. L.; Li, C. Z. Dynamically formed surfactant assembly at the electrified electrode-electrolyte interface boosting CO₂ electroreduction. *J. Am. Chem. Soc.* 2022, *144* (14), 6613-6622. DOI: 10.1021/jacs.2c02486.
- (52) Huang, Y.; Handoko, A. D.; Hirunsit, P.; Yeo, B. S. Electrochemical reduction of CO₂ using copper single-crystal surfaces: effects of CO* coverage on the selective formation of ethylene. *ACS Catal.* 2017, 7 (3), 1749-1756. DOI: 10.1021/acscatal.6b03147.
- (53) Luo, W.; Nie, X.; Janik, M. J.; Asthagiri, A. Facet dependence of CO₂ reduction paths on Cu electrodes. *ACS Catal.* 2016, 6 (1), 219-229. DOI: 10.1021/acscatal.5b01967.
- (54) Zheng, X. W.; Zhang, S. T.; Li, W. P.; Gong, M.; Yin, L. L. Experimental and theoretical studies of two imidazolium-based ionic liquids as inhibitors for mild steel in sulfuric acid solution. *Corrosion Science* 2015, *95*, 168-179. DOI: 10.1016/j.corsci.2015.03.012.
- (55) Basics of electrochemical impedance spectroscopy. Gamry Instruments, 2010. http://www.gamry.com/assets/Application-Notes/Basics-of-EIS.pdf (accessed 8/8/13).
- (56) Kern, P.; Landolt, D. Adsorption of organic corrosion inhibitors on iron in the active and passive state. A replacement reaction between inhibitor and water studied with the rotating quartz crystal microbalance. *Electrochim. Acta* 2001, 47 (4), 589-598. DOI: 10.1016/s0013-4686(01)00781-2.
- (57) Malkani, A. S.; Anibal, J.; Chang, X. X.; Xu, B. J. Bridging the gap in the mechanistic understanding of electrocatalysis via in situ characterizations. *Iscience* 2020, *23* (12). DOI: 10.1016/j.isci.2020.101776.

- (58) Heyes, J.; Dunwell, M.; Xu, B. CO₂ reduction on Cu at low overpotentials with surface-enhanced in situ spectroscopy. *J. Phys. Chem. C* 2016, *120* (31), 17334-17341. DOI: 10.1021/acs.jpcc.6b03065.
- (59) Dahl, K.; Sando, G. M.; Fox, D. M.; Sutto, T. E.; Owrutsky, J. C. Vibrational spectroscopy and dynamics of small anions in ionic liquid solutions. *The Journal of Chemical Physics* 2005, 123 (8), 084504. DOI: 10.1063/1.2000229 (accessed 2022/12/14).
- (60) Resasco, J.; Lum, Y.; Clark, E.; Zeledon, J. Z.; Bell, A. T. Effects of anion identity and concentration on electrochemical reduction of CO₂. *ChemElectroChem* 2018, *5* (7), 1064-1072. DOI: 10.1002/celc.201701316 (accessed 2019/05/17).
- (61) Goyal, A.; Marcandalli, G.; Mints, V. A.; Koper, M. T. M. Competition between CO₂ reduction and hydrogen evolution on a gold electrode under well-defined mass transport conditions. *J. Am. Chem. Soc.* 2020, *142* (9), 4154-4161. DOI: 10.1021/jacs.9b10061.
- (62) Sheng, W.; Zhuang, Z.; Gao, M.; Zheng, J.; Chen, J. G.; Yan, Y. Correlating hydrogen oxidation and evolution activity on platinum at different pH with measured hydrogen binding energy. *Nat. Commun.* 2015, *6* (1), 5848. DOI: 10.1038/ncomms6848.

TOC

